THE POTENTIAL OF A DIGITAL HYDRAULIC WINCH DRIVE SYSTEM

Sondre Nordås, Morten Kjeld Ebbesen, Torben Ole Andersen*
University of Agder
Jon Lilletunsvei 9, 4879 Grimstad, Norway
*Aalborg University
*Pontoppidanstraede 101, 9220 Aalborg East, Denmark
E-mail: sondre.nordas@uia.no, morten.k.ebbesen@uia.no, toa@et.aau.dk
Phone: +47 3723 3198

ABSTRACT

Digital hydraulic piston pumps and motors have shown the potential of improving efficiency in hydraulic systems. Two independently controlled fast switching on/off valves are connected to each piston chamber and allows for optimal valve timing and independent piston control. Each piston chamber is only pressurized when necessary, resulting in losses that almost scale with motor and pump displacement. This simulation study investigates the potential of using digital hydraulic pumps and motors to increase efficiency in a hydraulic offshore auxiliary winch with a safe working load equal to 20000 kg. One digital hydraulic winch drive system and one conventional hydraulic winch drive system are simulated hoisting two different loads. The payload in the first load case is 18000 kg and the payload in the second load case is 4000 kg. The efficiency and control performance of the two different winch drive systems are then evaluated. The simulation results show that digital hydraulic winch drive systems have the potential of increasing efficiency of hydraulic offshore winches.

KEYWORDS: Digital hydraulic pump/motor, hydraulic offshore winch, simulation, efficiency

1 INTRODUCTION

Hydraulic winches are widely used for various offshore lifting operations. They are for example used in cranes for deck to deck lifting operations, loading and unloading of supply vessels and subsea lifting operations, but they can also be used at the drill floor for small lifting operations.

The working environment on an offshore drilling unit is harsh and sets high requirements for all offshore equipment. The equipment should be light, small in volume and have a minimum of downtime. For example, every extra pound of weight increases the cost of structural material by 1 - 5$, the platform deck area has a value of approximately 600 - 6 000 $\$/ft^2$ and the cost of a production shutdown ranges from 37500 $\$/h$ for small

Gulf of Mexico platforms to 187500 $\$/h$ for large North Sea platforms [1]. Hydraulic actuation systems have normally been used, but because of environmental issues, more energy efficient systems are now required. Electric solutions tend to replace hydraulic solutions in rotational applications. Electrical solutions offer higher efficiency, no risk of oil leakage, high position accuracy, and few maintenance tasks [2]. The benefits of electric motors have to be weighed up against the key features of hydraulic systems. Key features of hydraulic motors and systems are for example high torque density, they can operate in stall conditions without damage, it is easy and efficient to store energy in accumulators, they are tolerant of shock loads due to the compressibility of the hydraulic oil, and the fluid carries away the generated heat to a heat exchanger placed at a convenient place [2]. New research has shown that in addition to the already mentioned benefits of hydraulic motors, the new digital hydraulic pump and motor technology also has the potential of designing highly efficient systems.

Digital hydraulic pump and motor technology can for example be applied to hydraulic hybrid buses and cars [3, 4], tidal current energy converters [5], hydraulic actuated booms [6, 7, 8], and wind turbines [9]. The piston chambers in a digital hydraulic pump (DHP) or a digital hydraulic motor (DHM) can be controlled individually to operate in pump, motor or idle mode. In idle mode, the low-pressure valve is kept open an entire shaft revolution. Hence, a piston chamber in idle mode is never pressurized and leakage losses and friction losses are therefore minimized. Displacement of a DHM is controlled by changing the ratio of pistons running in motor mode and idle mode resulting in losses that scales more with displacement compared to traditional variable displacement piston machines and allowing for high efficiency even at partial displacement.

2 SIMULATION MODEL

In this paper, two different winch drive systems are simulated, one conventional hydraulic winch drive system (CHWDS) and one digital hydraulic winch drive system (DHWDS). Both winch drive systems are driving the same winch drum with two different load cases. In the first load case, the payload is equal to 18000 kg and lifted 10 m. The velocity is ramped up to 1 m/s with a ramp time of 2 s. For the second load case, the payload is equal to 4000 kg and lifted 10 m. The velocity is ramped up to 1.5 m/s with a ramp time of 3 s. The two load cases are summarized in Tab. 1.

Table 1: Simulation parameters

	Load Case 1	Load Case 2
Mass of load	18000 kg	4000 kg
Hoisting distance	10 m	10 m
Max speed	1 m/s	1.5 m/s
Ramp time	2 s	3 s

2.1 Modeling of the Winch

Figure 1 shows all relevant winch elements. The winch has a drum capacity of 3600 m of wire and a safe working load of 20000 kg. In this study the inertia of the winch and wire wound onto the drum is assumed to be constant because the simulated traveling distance

is small compared to the total wire length. It is also assumed that only the outer wire layer is used. Hence the winch radius, r_{winch}, is considered to be constant. Neither friction in the drum nor elasticity in the wire are included.

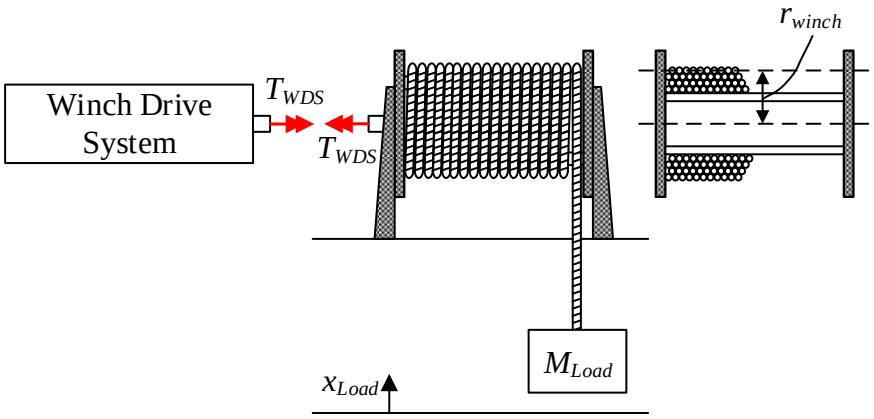

Figure 1: Simulated winch system

The equation of motion for the winch is shown in Eq. 1.

$$\ddot{\theta}_{drum} = \frac{T_{WDS} - M_{Load} \cdot g \cdot r_{winch}}{J_{eff}} \tag{1}$$

where T_{WDS} is the torque from the winch drive system acting on the drum, M_{Load} is the mass of the payload, g is acceleration of gravity, r_{winch} is the radius of the outer winch layer, and J_{eff} is the effective mass moment of inertia. The effective mass moment of inertia is calculated as shown in Eq. 2.

$$J_{eff} = M_{Load} \cdot r_{winch}^2 + J_{winch} + J_{WDS} \tag{2}$$

where J_{winch} includes the inertia of the drum and the wire wound onto the drum and J_{WDS} is the inertia of the drive system that is mechanically connected to the winch drum. The drive torque, T_{WDS}, for the two different winch drive systems are given in the following sections.

2.2 Modeling of the Conventional Hydraulic Winch Drive System

The conventional hydraulic winch drive system is a closed circuit system with one variable displacement over center axial piston pump delivering working fluid to two variable displacement axial piston motors. Figure 2 illustrates the simulated CHWDS. Line A is the high-pressure side of the motor and line B is the low-pressure side. In addition to the main pump, a smaller pump is installed to ensure that the pressure in line A and line B stays above 25 bar. This external circuit is modeled as a constant pressure source of 25 bar. The main axial piston pump has a displacement of 500 cc/rev and the two axial piston motors have a displacement of 250 cc/rev. The pump is driven at a constant velocity equal to 1800 rpm and can deliver pressure up to 350 bar.

The torque delivered to the winch drum from the drive system is calculated as shown in Eq. 3.

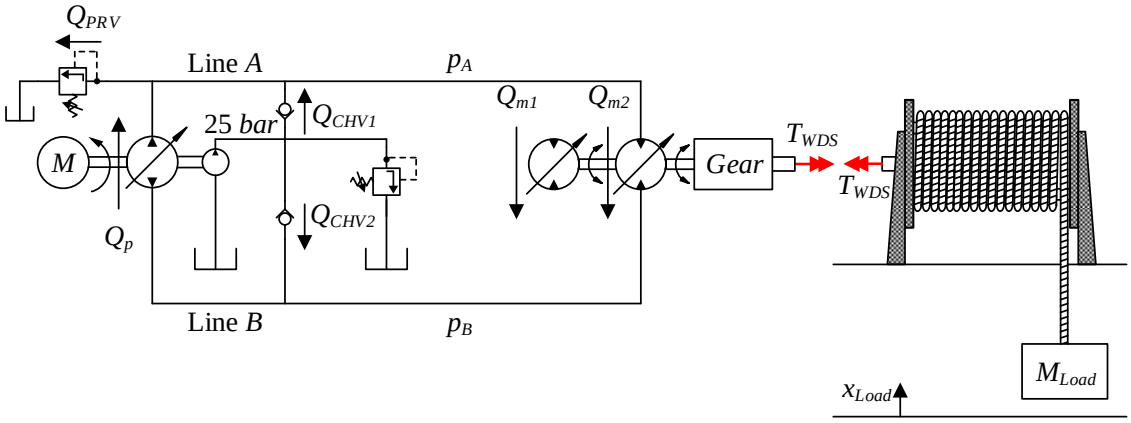

Figure 2: Conventional hydraulic winch drive system

$$T_{WDS} = 2 \cdot \frac{(p_A - p_B) \cdot V_{gm}}{2 \cdot \pi} \cdot i_{gear} \cdot n_{hmm} \cdot n_{gear} \tag{3}$$

where p_A is the pressure in line A, p_B is the pressure in line B, V_{gm} is the common displacement of the motors, i_{gear} is the gear ratio, n_{hmm} is the hydromechanical efficiency of the motors, and n_{gear} is the efficiency of the gear box. The hydromechanical efficiency is found by linear interpolation between measured data for a representative axial piston motor. The pressure in line A and line B is calculated by integrating the pressure gradients calculated as shown in Eq. 4 and Eq. 5 respectively.

$$\dot{p}_A = \frac{\beta}{V_A} \cdot (Q_p - Q_{PRV} + Q_{CHV1} - Q_m) \tag{4}$$

$$\dot{p}_B = \frac{\beta}{V_B} \cdot (Q_m + Q_{CHV2} - Q_p) \tag{5}$$

where β is the bulk modulus of the oil, V_A and V_B are the volume in line A and B respectively, Q_p is the pump flow, Q_m is the total motor flow ($Q_m = Q_{m1} + Q_{m2}$), Q_{PRV} is the flow through the pressure relief valve connected to line A, Q_{CHV1} and Q_{CHV2} are the flows through the two check valves.

The following equations describe the flow through the pump and the motors:

$$Q_p = \frac{\dot{\theta}_p \cdot V_{gp}}{2 \cdot \pi} \cdot n_{vp} \tag{6}$$

$$Q_m = 2 \cdot \frac{\dot{\theta}_m \cdot V_{gm}}{2 \cdot \pi} \cdot \frac{1}{n_{vm}} \tag{7}$$

where $\dot{\theta}_p$ is the speed of the pump, V_{gp} is the pump displacement, n_{vp} is the volumetric efficiency of the pump, n_{vm} is the volumetric efficiency of the motors, and $\dot{\theta}_m$ is the speed of the motors.

The dynamic response of the swash plate for the axial piston pump and motors is described by a first order system as shown in Eq. 8.

$$\dot{V}_g = \frac{V_g - V_{gc}}{\tau} \tag{8}$$

where V_g is the current displacement, V_{gc} is the desired displacement and τ is the time constant.

2.2.1 Control system

The control system for the CHWDS is divided into two different control systems, one for the motors and one for the pump. The motors have a simple open-loop controller, and the pump has a feedforward controller and a feedback controller. The desired motor displacement is calculated based on a measured value of the load, a reference acceleration of the winch drum and a desired pressure drop across the motor as shown in Eq. 9.

$$V_{gmc} = \frac{(\ddot{\theta}_{ref} \cdot J_{eff} + \widetilde{M}_{Load} \cdot g \cdot r_{winch}) \cdot 2 \cdot \pi}{\Delta p_m \cdot i_{gear}} \cdot 0.5 \tag{9}$$

where $\ddot{\theta}_{ref}$ is the reference acceleration for the winch drum, $\widetilde{M}_{Load}$ is the measured value of the payload and Δp_m is the desired pressure drop across the motors.

The pump has a position feed-back controller and a flow feed-forward controller as shown in Fig. 3

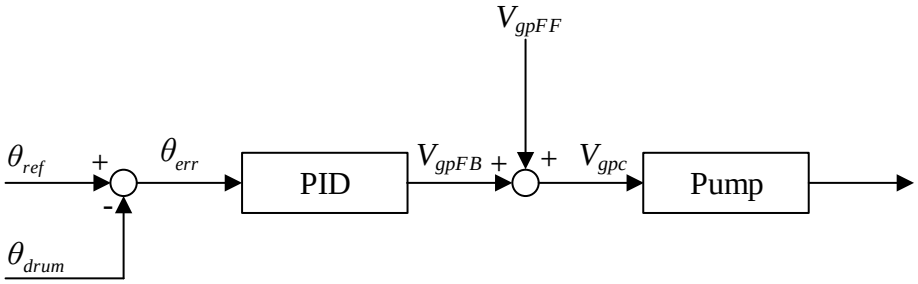

Figure 3: Pump controller

Assuming that the volumetric efficiency for the pump is equal to one, the feed-forward pump displacement is calculated by rearranging Eq. 6 as shown in Eq. 10.

$$\begin{aligned} Q_{ref} &= \frac{V_{gpFF} \cdot \dot{\theta}_p}{2 \cdot \pi} \\ &\Downarrow \\ V_{gpFF} &= \frac{2 \cdot \pi \cdot Q_{ref}}{\dot{\theta}_p} \\ &= \frac{2 \cdot \pi \left(\frac{\dot{\theta}_{ref} \cdot i_{gear} \cdot V_{gmc}}{2 \cdot \pi} \right) \cdot 2}{\dot{\theta}_p} \\ &= \frac{\dot{\theta}_{ref} \cdot i_{gear} \cdot V_{gmc} \cdot 2}{\dot{\theta}_p} \end{aligned} \tag{10}$$

where $\dot{\theta}_{ref}$ is the reference velocity of the winch drum and $\dot{\theta}_p$ is the pump speed. The feed-back control signal is calculated as shown in Eq. 11

$$V_{gpFB} = \theta_{err} \cdot k_p + \dot{\theta}_{err} \cdot k_d + \int \theta_{err} \cdot k_i \; dt \tag{11}$$

where θ_{err} is the position error of the winch drum and k_p, k_d and k_i are the controller gains for the PID-controller. Finally the desired pump displacement is calculated as shown in Eq. 12.

$$V_{gpc} = V_{gpFF} + V_{gpFB} \tag{12}$$

2.3 Modeling of the Digital Hydraulic Winch Drive System

The digital hydraulic winch drive system consists of a DHP, DHM, and two gas accumulators connected in a closed circuit system, as shown in Fig. 4. The DHP is driven by an electrical motor running at a constant velocity of 1800 *rpm*. The DHM is directly connected to the winch drum without a gear box. The DHP and the DHM are two radial piston units with respectively 9 and 42 cylinders. Both units are controlled by using sequential flow diverting strategy, meaning that the entire cylinder displacement has to be used when selecting pump or motor mode. The on/off valves are only switched when the piston is close to top dead center (TDC) and bottom dead center (BDC) when the flow is low. The actuation is timed in conjunction with the piston movement to minimize the pressure difference when switching the valves. This maximizes the efficiency and minimizes pressure peaks and flow peaks. The two gas accumulators are used to smooth out the pressure and flow peaks in line *A* and *B*.

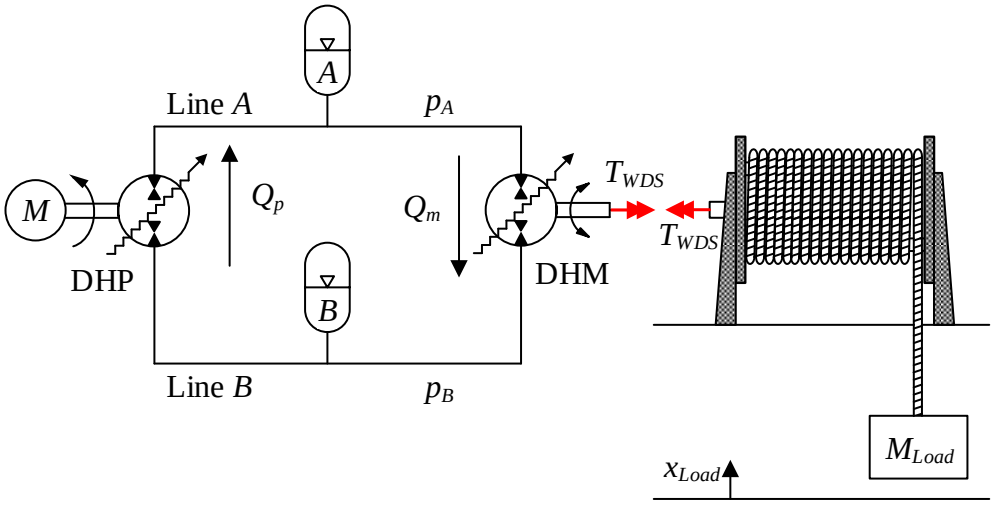

Figure 4: Digital hydraulic winch drive system

2.3.1 Modeling of the Digital Hydraulic Pump and Motor

It is assumed that the cylinder configuration is the same for both the DHP and the DHM. For simplicity, only calculations for one of the pistons in the DHM are shown in this section, but the same method is used for all of the pistons, both for the DHM and DHP.

The contribution from all the cylinders are summed up in Eq. 20..22. The on/off valves are assumed to be leak free, and the DHP and DHM models do not include any friction or leakage.

Figure 5 shows the cylinder configuration for one cylinder. The continuity equation is used to calculate the pressure gradient in the cylinder as shown in Eq. 13.

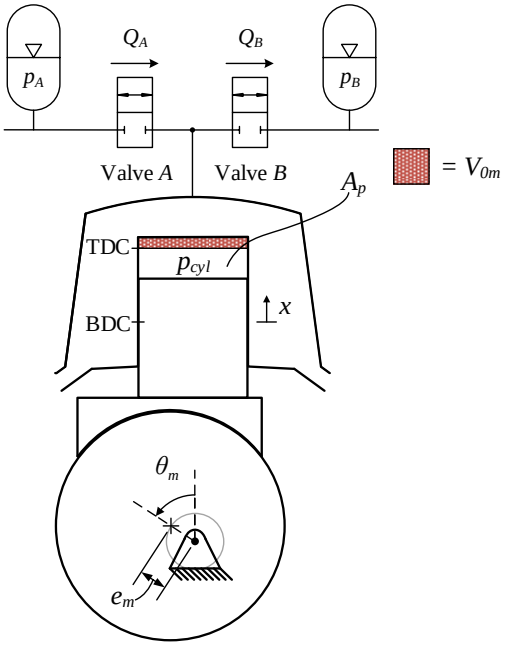

Figure 5: Cylinder configuration of one cylinder with $\theta_m = \pi/4$

$$\dot{p}_{cyl} = \frac{\beta}{V_{cyl}} \cdot \left(Q_A - Q_B - \dot{V}_{cyl}\right) \tag{13}$$

where β is the effective bulk modulus of the oil, V_{cyl} is the cylinder volume, Q_A and Q_B is the flow through valve A and B, and $\dot{V}_{cyl}$ is the rate of change in cylinder volume. $\dot{V}_{cyl}$ is positive if the volume is expanding. The cylinder volume is calculated as shown in Eq. 14 and the rate of change in cylinder volume is calculated as shown in Eq. 15.

$$V_{cyl} = V_{0m} + \frac{V_{dm}}{2} \cdot (1 - \cos(\theta_m)) \tag{14}$$

$$\dot{V}_{cyl} = \frac{V_{dm}}{2} \cdot \sin(\theta_m) \cdot \dot{\theta}_m \tag{15}$$

where V_{0m} is the dead volume in the cylinder and V_{dm} is the discharge volume of the cylinder. The volume flow through the on/off valves, Q_A and Q_B, are calculated by Eq. 16 and Eq. 17 respectively.

$$Q_A = \frac{u_A}{k_f} \cdot \sqrt{p_A - p_{cyl}} \cdot sign(p_A - p_{cyl}) \tag{16}$$

$$Q_B = \frac{u_B}{k_f} \sqrt{p_{cyl} - p_B} \cdot sign(p_{cyl} - p_B) \tag{17}$$

where k_f is the flow coefficient of the valves, and u_A and u_B are the opening ratios of the valves ranging from 0 to 1, where 0 is fully closed and 1 is fully open. Valve A and B

have the same flow coefficient and the same dynamic response. The dynamic response is described by the second order system shown in Eq. 18.

$$\ddot{u} = u_{con} \cdot \omega^2 - u \cdot \omega^2 - 2 \cdot \zeta \cdot \omega \cdot \dot{u} \tag{18}$$

where u_{con} is the control signal, ζ is the damping ratio and ω is the natural frequency. The control signal is either 0 or 1. The torque contribution from one cylinder is calculated as shown in Eq. 19

$$T_{cyl} = p_{cyl} \cdot A_p \cdot e_m \cdot \sin(\theta_m) \tag{19}$$

Finally, the total motor torque and the total flow in and out of the DHM is calculated as the sum of the contribution from all pistons, as shown below in Eq. 20, 21 and 22 respectively.

$$T_{WDS} = \sum_{i=1}^{42} T_{cyl,i} \tag{20}$$

$$Q_{inm} = \sum_{i=1}^{42} Q_{A,i} \tag{21}$$

$$Q_{outm} = \sum_{i=1}^{42} Q_{B,i} \tag{22}$$

2.3.2 Valve Parameters

The fast switching on/off valve is by far the most critical element in digital hydraulic machines. Some important features are; high durability, low cost, low power consumption, zero or low leakage, and compact design [10]. Simulations and experimental results presented in [11] show that valve throttling losses are one of the major energy dissipative sources for hydraulic motors and that valve timing has a significant impact on valve throttling losses. The valves must, therefore, have high accuracy, high flow rate and low switching time. In [12], Daniel B. Roemer et al. developed an expression for the efficiency of a DHM as a function of a normalized valve switching time, $\bar{t}_s$, and a normalized valve flow coefficient, $\bar{k}_f$. The normalized valve parameters were defined as shown in Eq. 23 and 24.

$$\bar{t}_s = \frac{t_s}{T_{rev}} \quad \text{with} \quad T_{rev} = \frac{2 \cdot \pi}{\dot{\theta}_{max}} \tag{23}$$

$$\bar{k}_f = \frac{k_f}{\sqrt{\Delta p}/Q_{mean}} \quad \text{with} \quad Q_{mean} = \frac{V_d}{\pi/\dot{\theta}_{max}} \tag{24}$$

Figure 6 shows the motor efficiency as a function of the normalized switching time and the normalized flow coefficient.

Using the results from Fig. 6 and selecting the normalized flow coefficient and the normalized switching time to be 4 %, the target efficiency at 20 % displacement is 97 %. By rearranging Eq. 23 and 24 the valve switching time and the valve flow coefficient is calculated as shown below in Eq. 25 and 26 respectively.

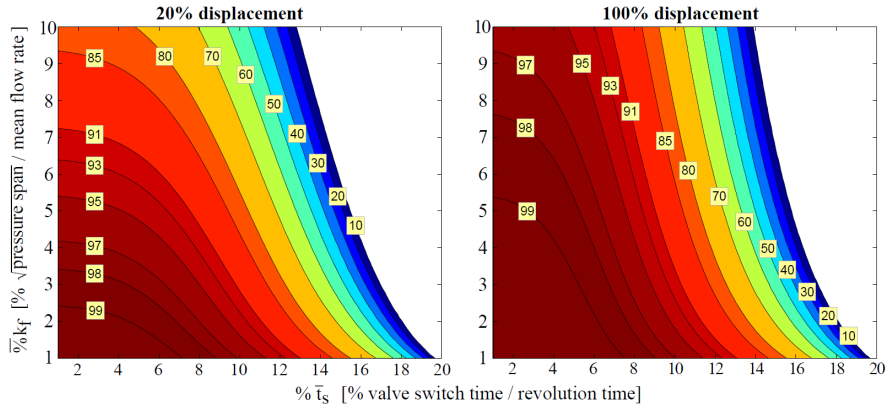

Figure 6: Motor efficiency as a function of normalized valve switching time and normalized valve flow coefficient [13]

$$
\begin{aligned}
\bar{t}_s &= \frac{t_s}{T_{rev}} \quad \text{with} \quad T_{rev} = \frac{2 \cdot \pi}{\dot{\theta}_{max}} \\
&\Downarrow \\
t_s &= \bar{t}_s \cdot T_{rev} \\
&= \bar{t}_s \cdot \frac{2 \cdot \pi}{\dot{\theta}_{max}}
\end{aligned} \tag{25}
$$

$$
\begin{aligned}
\bar{k}_f &= \frac{k_f}{\sqrt{\Delta p}/Q_{mean}} \quad \text{with} \quad Q_{mean} = \frac{V_d}{\pi/\dot{\theta}_{max}} \\
&\Downarrow \\
k_f &= \bar{k}_f \cdot \sqrt{\Delta p}/Q_{mean} \\
&= \bar{k}_f \cdot \frac{\sqrt{\Delta p} \cdot \pi}{V_d \cdot \dot{\theta}_{max}}
\end{aligned} \tag{26}
$$

The calculated flow coefficient and the switching time for the on/off valves for both the DHP and DHM are listed in Tab. 2.

Table 2: Valve parameters

	k_f	t_s
DHM	251560 $\frac{\sqrt{\Delta p}}{m^3/s}$	240 ms
DHP	53666 $\frac{\sqrt{\Delta p}}{m^3/s}$	1.3 ms

2.3.3 Pressure dynamics in line *A* and line *B*

For simplicity, only the calculation for the pressure gradient in line A is shown, but the pressure gradient in line B is calculated in the same manner. The pressure gradient in line A is calculated as shown in Eq. 27

$$\dot{p}_A = \frac{\beta}{V_A} \cdot (Q_{outp} - Q_{inm} - \dot{V}_{accA}) \tag{27}$$

where V_A is the volume in line A and accumulator A, Q_{outp} is the flow out of the pump, Q_{inm} is the flow into the motor and $\dot{V}_{accA}$ is the rate of change of accumulator volume. $\dot{V}_{accA}$ is positive if the volume is expanding and is calculated as shown below in Eq. 28.

$$\dot{V}_{accA} = \dot{p}_A \cdot \frac{V_{accAg}}{n_{accA} \cdot p_A} \tag{28}$$

where V_{accAg} is the gas volume in accumulator A and n_{accA} is the polytropic exponent for accumulator A. Eq. 28 is substituted into Eq. 27 and rearranged as shown in Eq. 29.

$$\dot{p}_A = \frac{\beta}{V_A} \cdot \frac{(Q_{outp} - Q_{inm})}{1 + \frac{\beta \cdot V_{accAg}}{V_A \cdot n_{accA} \cdot p_A}} \tag{29}$$

2.3.4 Control System

The control system for the DHWDS is divided into two, one for the pump and one for the motor. In general, the motor has an open loop torque controller which calculates motor displacement based on load measurements and a desired pressure drop across the motor. The pump has a displacement controller where the displacement is calculated based on the winch drum reference position and the known motor displacement. The pump also has a position feedback controller.

Motor Controller
To ensure a relatively smooth motor output torque, the 42 cylinder piston motor is divided into 14 banks, each with 3 pistons spaced equally around the shaft. The number of active banks, also called n_{step}, is calculated based on measurements of the payload, $\widetilde{M}_{Load}$, and a desired pressure drop across the motor, Δ_{pref}, as shown in Eq. 30.

$$n_{step} \approx \frac{\widetilde{M}_{Load} \cdot g \cdot r_{winch}}{\Delta p_{ref} \cdot T_{step}}, \quad \text{round of to nearest integer} \tag{30}$$

$n_{step} = 1$ corresponds to one active bank, $n_{step} = 2$ corresponds to two active banks and so on. Δp_{ref} is the desired pressure drop across the motor and T_{step} is the torque delivered by one active bank with a pressure drop across the motor equal to 1 Pa.

Pump Controller
The pump controller is based on the displacement controller first introduced in [14]. The DHM is directly connected to the drum, and the position reference of the drum is converted into a volume reference, V_{ref}, according to the motor displacement. Then the volume that already has been discharged from the pump, V_{est}, is calculated. The controller also has a position feedback controller, V_{err}, and compensates for the change of volume in accumulator A. Figure 7 illustrates the DHP controller and the pump mode decision, D, is calculated as shown in Eq. 31

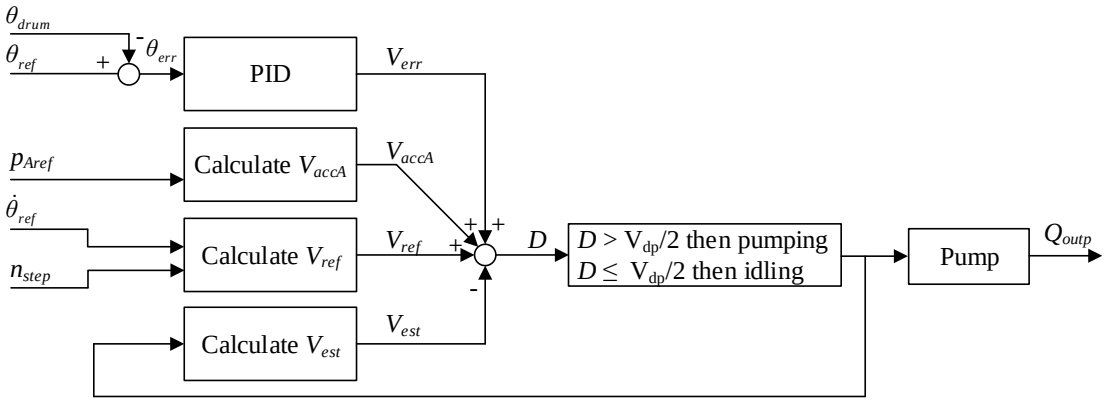

Figure 7: Pump controller

$$D = V_{ref} + V_{accA} + V_{err} - V_{est}, \;\rightarrow\; \begin{cases} \text{pumping} & \text{if} \quad D > V_{dp}/2 \\ \text{idling} & \text{if} \quad D \leq V_{dp}/2 \end{cases} \tag{31}$$

where $D > V_{dp}/2$ means that the estimated volume discharged from the pump is a half piston discharge volume smaller than the desired volume and that the next cylinder will operate in pump mode. $D \leq V_{dp}/2$ means that the estimated volume discharged from the pump is greater then the needed volume and that the next cylinder will run in idle mode. V_{ref} is calculated by integrating Eq. 32.

$$\dot{V}_{ref} = \frac{V_{dm} \cdot n_{step} \cdot 3 \cdot \dot{\theta}_{ref}}{2 \cdot \pi} \tag{32}$$

where $\dot{\theta}_{ref}$ is the speed reference of the winch drum. The estimated discharge volume, V_{est}, is calculated by the following equation.

$$V_{est} = n_{pump} \cdot V_{dp} \tag{33}$$

where n_{pump} is the total number of cylinders that already have been pumping and V_{dp} is the discharge volume of one of the pistons in the pump. The compression volume is not taken into account in Eq. 33, but can be included. The small error introduced by excluding the compression volume will in this control system be compensated for in the PID-controller. V_{accA} is calculated in Eq. 34.

$$V_{accA} = \frac{(p_{Aref} - p_{A0}) \cdot V_{accAg0}}{n_{accA} \cdot p_{A0}} \tag{34}$$

where p_{A0} is the initial pressure in line A, V_{gA0} is the gas volume in accumulator A at the initial pressure p_{A0} and p_{Aref} is the reference pressure in line A. p_{Aref} is calculated as shown below in Eq. 35.

$$p_{Aref} = \frac{\ddot{\theta}_{ref} \cdot J_{eff} + \widetilde{M}_{Load} \cdot g \cdot r_{winch}}{T_{step} \cdot n_{step}} + p_{B0} \tag{35}$$

where p_{B0} is the initial pressure in line B. V_{err} is the output signal from the PID-controller and is calculated as shown in Eq. 36

$$V_{err} = \theta_{err} \cdot k_p + \dot{\theta}_{err} \cdot k_d + \int \theta_{err} \cdot k_i \; dt \tag{36}$$

where θ_{err} is the difference of the reference drum position and the actual drum position and k_p, k_d and k_i are the control parameters in the PID-controller .

3 SIMULATION RESULTS

In this section the simulation results are presented. The same control parameters are used in the conventional winch drive controller and the digital hydraulic winch drive controller for both load case 1 and load case 2. The control parameters for the CHWDS are as follows: $\Delta p_{ref} = 225\ bar$, $p_{B0} = 25\ bar$, $k_p = 7 \cdot 10^{-4}\ m^3$, $k_d = 2 \cdot 10^{-4}\ m^3 s$ and $k_i = 5 \cdot 10^{-3}\ m^3/s$. The control parameters for the DHWDS are as follows: $\Delta p_{ref} = 225\ bar$, $p_{B0} = 25\ bar$, $k_p = 0.1\ m^3$, $k_d = 0.025\ m^3 s$, and $k_i = 0.2\ m^3/s$.

3.1 Load Case 1

In load case 1 the payload is equal to 18000 kg and the speed is ramped up to 1 m/s with a ramp time of 2 s. Figure 8 and 9 show the simulation results of the CHWDS, left hand side, and the DHWDS, right hand side.

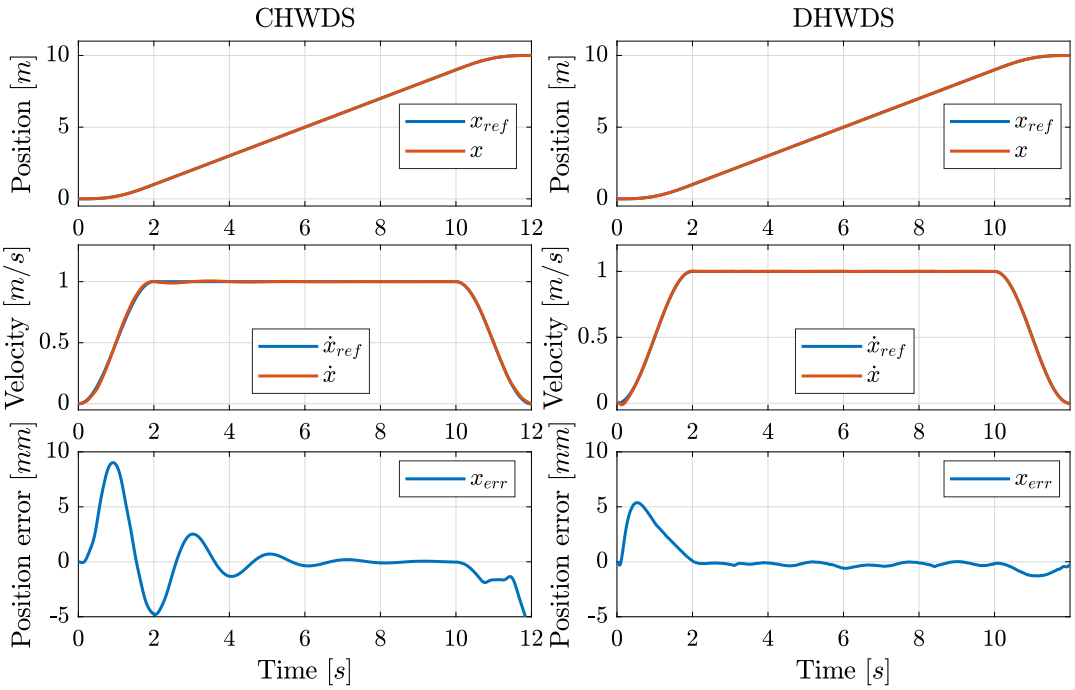

Figure 8: Simulation results position and velocity tracking in load case 1

The sub-plots from top to bottom in Fig. 8 show the simulated payload position together with the reference position, the load speed together with the reference speed and finally the position error. The simulated payload position and speed follow their references well, both for the CWDS and the DHWDS. Maximum position error occurs when

accelerating the load and is 9 *mm* for the CHWDS and 5.4 *mm* for the DHWDS. The position error for the CHWDS converges toward zero when the winch runs with constant speed and the error for the DHWDS oscillates around zero with a small amplitude.

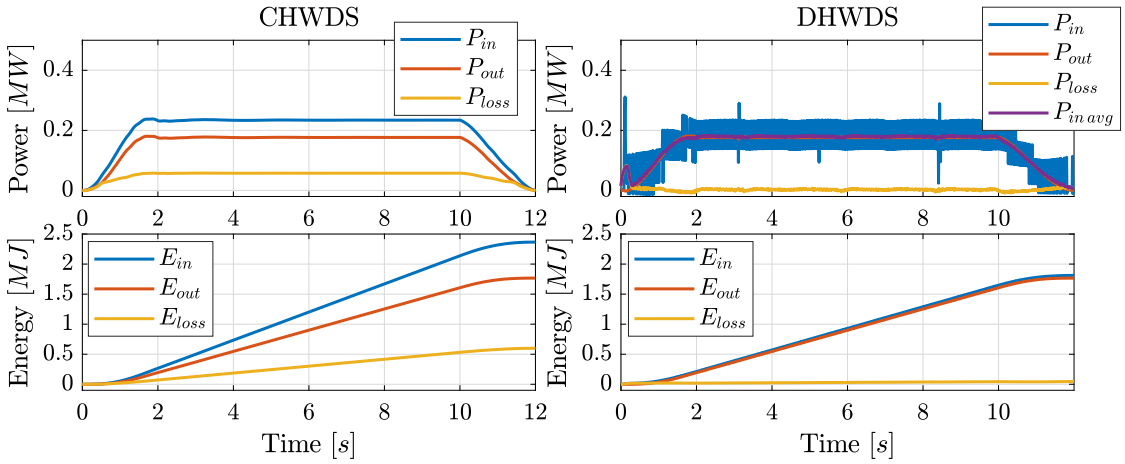

Figure 9: Simulation results for power and energy consumption in load case 1

The top sub-plots in Fig. 9 show the input power, output power and the power losses of the hydraulic system. On the right hand side, a moving average filter is also included. The moving average filter takes the average of the input power during a period of 0.2 *s*. The bottom sub-plots show the consumed energy together with the output energy and energy losses.

When driving with constant speed of 1 m/s and a payload equal to 18000 *kg*, the input power to the CHWDS is approximately 234 *kW* and the output power is approximately 176 *kW*, resulting in loss equal to 58 *kW*. The input power to the DHWDS is heavily oscillating because of the nature of the DHP. The DHP enables and disables pistons on a stroke by stroke basis which results in input power oscillations. The same peaks occur in the pump flow, but the accumulators connected to line *A* and *B* smooth out the peaks. The mean input power to the DHWDS when operating at constant speed is 181 *kW* and the mean loss is only 5 *kW*.

In the bottom sub-plots in Fig. 9, it is easy to see that the energy losses are much greater for the CHWDS than for the DHWDS. The total energy consumed by the CHWDS is 2365 *kJ* and the loss is 599 *kJ* which results in a total system efficiency equal to 75 %. The total system efficiency for the DHWDS is 97 % where the total consumed energy is 1813 *kJ* and the total energy loss is only 47 *kJ*.

3.2 Load Case 2

In load case 2 the payload is equal to 4000 *kg* and the speed is ramped up to 1.5 m/s with a ramp time of 3 *s*. Figure 10 and 11 show the simulation results of the CHWDS, left hand side, and the DHWDS, right hand side.

Figure 10 shows that both drive systems follow their position and speed references well. The position error for the CHWDS tends to oscillate when accelerating or decelerating the load but stabilizes around zero when running at constant speed. The maximum position error for the CHWDS is -8.4 *mm* and only -1.6 *mm* for the DHWDS. The small oscillations shown in the position error for the DHWDS in load case 1 can also be seen in load case 2.

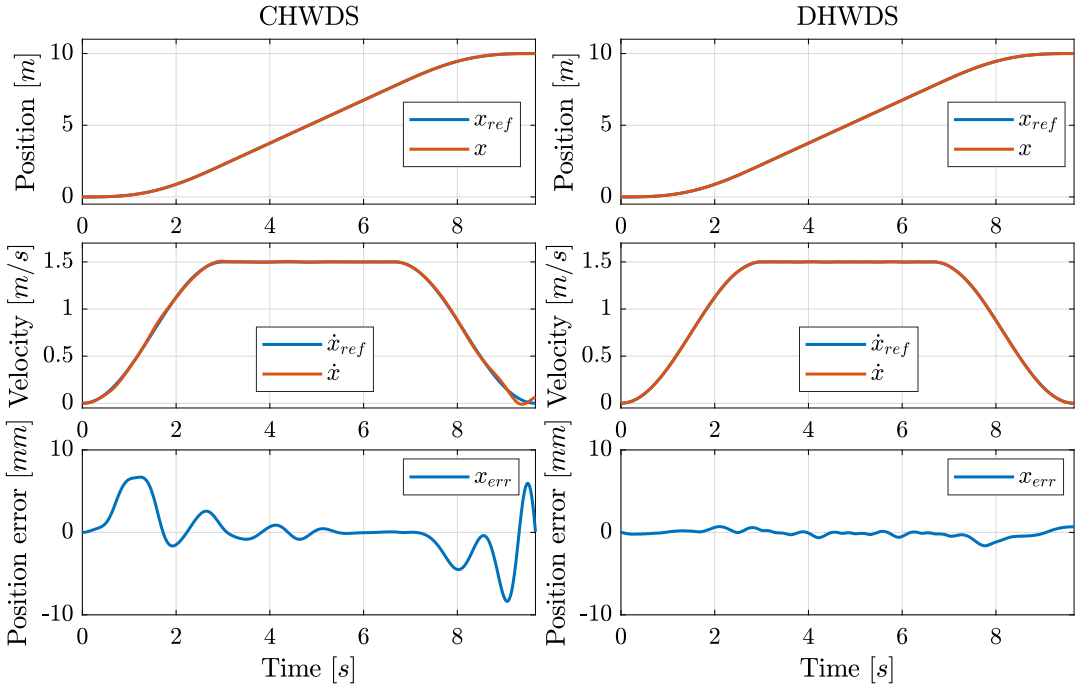

Figure 10: Simulation results position and velocity tracking in load case 2

Figure 11 shows that the input power to the CHWDS is approximately 112 *kW* and the output power is 59 *kW* when driving with a constant speed of 1.5 m/s. For the DHWDS the input power is heavily oscillating, but the mean value is approximately 61 *kW*. The total consumed energy for the simulated trajectory is 769 *kJ* for the CHWDS and only 417 *kJ* for the DHWDS. The losses are 377 *kJ* for the CHWDS and only 25 *kJ* for the DHWDS. This gives a total efficiency for the entire simulated trajectory equal to 51 % for the CHWDS and 94 % for the DHWDS.

3.3 Discussion

In this section, the presented results are summarized and further discussed. Some of the most important results are summarized in Tab. 3

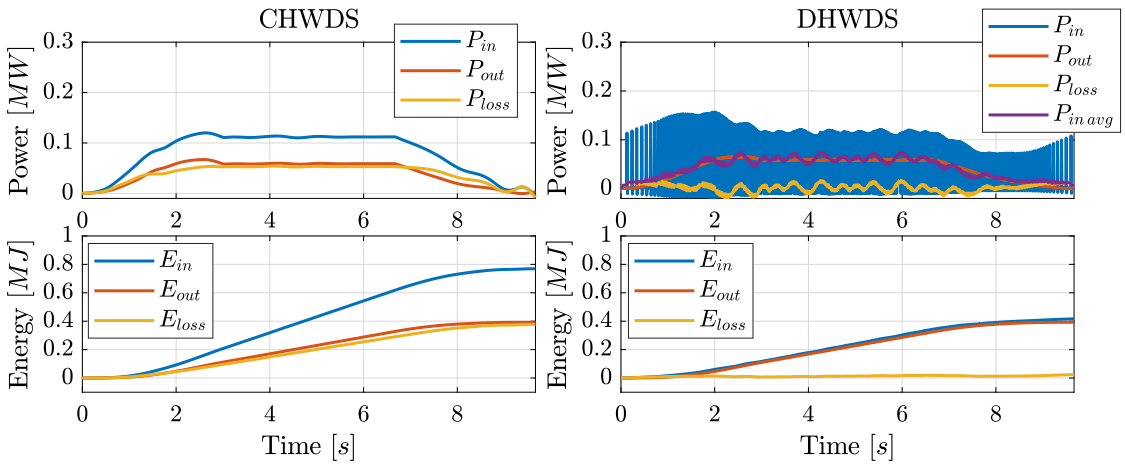

Figure 11: Simulation results for power and energy consumption in load case 2

Table 3: Summarized results

	Load case 1		**Load case 2**	
	CHWDS	DHWDS	CHWDS	DHWDS
Input power at constant speed	234 *kW*	181 *kW*	112 *kW*	61 *kW*
Power losses at constant speed	58 *kW*	5 *kW*	50 *kW*	1 *kW*
Total energy consumed	2365 *kJ*	1813 *kJ*	769 *kJ*	417 *kJ*
Total energy losses	599 *kJ*	47 *kJ*	377 *kJ*	25 *kJ*
Total efficiency	75 %	97 %	51 %	94 %
Max position error	9 *mm*	5.4 *mm*	-8.4 *mm*	-1.6 *mm*

The total system efficiency for the CHWDS is 75 % in load case 1 and 51 % in load case 2 and the maximum position error is 9 *mm* and -8.4 *mm* respectively. The CHWDS has higher efficiency when operating with higher loads. The same tendency can be observed for the DHWDS, but the change in efficiency is not that big. When reducing the load from 18000 *kg* down to 4000 *kg*, the efficiency of the CHWDS is reduced by 32 % and for the DHWDS, the efficiency is only reduced by 3 %. When operating with constant speed, the position error for the CHWDS tends to converge towards zero, while the position error for the DHWDS tends to oscillate with a small amplitude. These small oscillations are affected by control parameters, accumulator properties and the number of pistons in the DHP and the DHM.

The DHWDS consumes approximately 550 *kJ* less than the CHWDS when operating load case 1. If the same load were supposed to be hoisted 3000 *m*, the DHWDS would use 165 *MJ* less energy than the CHWDS. For one short lifting operation, the saved energy is not that much, but for a winch that is frequently used over time and with high lifting operations, the savings can be significant.

This study shows that there is a significant improvement in efficiency when using the DHWDS. Neither leakage and friction losses in the DHP and the DHM nor power consumption of the on/off valves are included in this study. The real efficiency will therefore most likely be lower than for the simulated system. Because the increase in efficiency is so high, especially when operating small loads, and knowing that previous studies show that digital hydraulic units have high efficiency for a wide range of operations [15], it is realistic to expect that the efficiency for the DHWDS will remain significantly higher than CHWDS even when all losses are included.

4 CONCLUSION

This simulation study compares the efficiency and controllability of a CHWDS and a DHWDS. Each winch drive system is simulated hoisting two different loads, one large load and one small load. The simulation results show that the system efficiency for the DHWDS was significantly higher than for the CHWDS, especially when operating small loads. This study shows that DHWDS has the potential of increasing efficiency in hydraulic winches while the controllability remains high.

References

[1] M. L. Christensen and L. Zimmer, “Optimization of offshore electric power systems,” *IEEE Transactions on Industry Applications*, 1986.

[2] W. Pawlus, M. Choux, and M. R. Hansen, "Hydraulic vs. electric: A review of actuation systems in offshore drilling equipment," *Modeling, Identification and Control*, vol. 37, no. 1, pp. 1–17, 2016.

[3] K. Rydberg, "Energy efficient hydraulic hybrid drives," *The 11th Scandinavian International Conference on Fluid Power, Lindköping, Sweden*, June 2009.

[4] J. Taylor, W. Rampen, D. Abrahams, and A. Latham, "Demonstration of a digital displacement hydraulic hybrid bus," *JSAE Annual Congress, Yokohama, Japan*, May 2015.

[5] G. S. Payne, A. E. Kiprakis, M. Ehsan, W. H. S. Rampen, J. P. Chik, and A. R. Wallace, "Efficiency and dynamic performance of digital displacement^{TM} hydraulic transmission in tidal current energy converters," *Proceedings of the Institution of Mechanical Engineers, Part A: Journal of Power and Energy*, vol. 221, no. 2, pp. 207–218, 2007.

[6] M. Karvonen, M. Heikkilä, M. Huova, M. Linjama, and K. Huhtala, "Simulation study - improving efficiency in mobile boom by using digital hydraulic power management system," *The 12th Scandinavian International Conference on Fluid Power, Tampere, Finland*, pp. 355–368, May 2011.

[7] M. Heikkilä and M. Linjama, "Hydraulic energy recovery in displacement controlled digital hydraulic system," *The 13th Scandinavian International Conference on Fluid Power, Linköping, Sweden*, pp. 513–519, June 2013.

[8] M. Heikkilä, M. Karvonen, M. Linjama, S. Tikkanen, and K. Huhtala, "Comparison of proportional control and displacement control using digital hydraulic power management system," *ASME/BATH 2014 Symposium on Fluid Power & Motion Control, Bath, United Kingdom*, September 2014.

[9] M. Sasaki, A. Yuge, T. Hayashi, H. Nishino, M. Uchida, and T. Noguchi, "Large capacity hydrostatic transmission with variable displacement," *The 9th International Fluid Power Conference, Aachen, Germany*, vol. 9, March 2014.

[10] B. Winkler, A. Plöckinger, and R. Scheidl, "State of the art in digital valve technology," *The 7th Workshop on Digital Fluid Power, Linz, Austria*, pp. 151–163, February 2015.

[11] H. Tian and J. D. Van de Ven, "Experimental study of the influence of valve timing on hydraulic motor efficiency," *ASME/BATH 2015 Symposium on Fluid Power & Motion Control, Chicago, Illinois, USA*, pp. 151–163, October 2015.

[12] D. Rømer, P. Johansen, H. C. Pedersen, and T. O. Andersen, "Analysis of valve requirements for high-efficiency digital displacement fluid power motors," in *8th International Conference on Fluid Power Transmission and Control, ICFP 2013*, pp. 122–126, World Publishing Cooperation, 2013.

[13] D. B. Roemer, *Design and optimization of fast switching valves for large scale digital hydraulic motors*. PhD thesis, Department of Energy Technology, Aalborg University, 2014.

[14] M. Heikkilä and M. Linjama, "Direct connection of digital hydraulic power management system and double acting cylinder-a simulation study," *The Fourth Workshop on Digital Fluid Power, Linz, Austria*, September 2011.

[15] W. Rampen, "Gearless transmissions for large wind turbines - the history and future of hydraulic drives," 2006. URL `http://www.artemisip.com/wp-content/uploads/2016/03/2006-11-Gearless-Transmissions-Bremen.pdf`.